Stanford Exploration Project, Report 112, November 11, 2002, pages 237–259

Dispersion of waves in porous cylinders with patchy saturation

James G. Berryman,[1] *Steven R. Pride*[2]

ABSTRACT

Laboratory experiments on wave propagation through saturated and partially saturated porous media have often been conducted on porous cylinders that were initially fully saturated and then allowed to dry while continuing to acquire data on the wave behavior. Since it is known that drying typically progresses from outside to inside, a sensible physical model of this process is concentric cylinders having different saturation levels — the simplest example being a fully dry outer cylindrical shell together with a fully wet inner cylinder. We use this model to formulate the equations for wave dispersion in porous cylinders for patchy saturation (*i.e.*, drainage) conditions. In addition to multiple modes of propagation obtained numerically from these dispersion relations, we find two distinct analytical expressions for torsional wave modes. We solve the dispersion relation for torsional waves for two examples: Massillon sandstone and Sierra White granite. The drainage analysis appears to give improved agreement with the data for both these materials.

INTRODUCTION

The classic work of Pochhammer (1876) and Chree (1886) gave exact solutions for wave propagation in elastic rods. When the rod is instead a porous cylinder with fluid-filled pores, the equations of linear elasticity do not describe all possible motions of the fluid/porous-solid mixture. Biot's theory of fluid-saturated porous media provides a continuum theory, permitting the fluid and solid components to move independently and accounts approximately for the attenuation of waves due to viscous friction. Gardner (1962) used Biot's theory (Biot, 1956a,b) to study long-wavelength extensional waves in circular cylinders. Gardner considered only the low-frequency regime where the second bulk compressional mode predicted by Biot's theory is diffusive in character. Gardner also limited consideration to the case of open-pore surface boundary conditions.

The present work is based in part on another paper by Berryman (1983), in which both open-pore and closed-pore surface boundary conditions for the fluid-saturated porous cylinder were studied. Here we consider only the open-pore surface, but we allow non-uniform or patchy saturation (Berryman, 1988; Knight and Nolen-Hoeksema, 1990; Knight *et al.*, 1998; Johnson, 2001) inside the cylinder. In particular, it is quite common to study partial satura-

[1]**email**: berryman@sep.stanford.edu
[2]**email**: spride@univ-rennes1.fr

tion in the laboratory under drainage or drying conditions wherein an initially fully saturated porous cylinder is allowed to dry while continuing to acquire data on the cylinder's modes of oscillation. We want to model this behavior explicitly. The simplest such model is concentric cylinders with a fully dry outer cylindrical shell enclosing a fully liquid-saturated inner cylinder. A more realistic model would involve many layers with various degrees of partial saturation between the dry outer shell and the saturated inner cylinder, but such complications will not be treated here. We find that studies of the two-layer case have all the important physical complications expected in this problem, while still having enough simplicity that some of the analysis can be done semi-analytically — thereby providing soughtafter insight into the problem.

We present the equations of poroelasticity, and then show the forms of the equations needed for cylindrical geometry. Appropriate boundary conditions for our problem are discussed. Equations are subsequently formulated to determine both the extensional and torsional modes of concentric poroelastic cylinders under conditions of partial saturation. Solutions of these equations are computed and discussed here for torsional waves, while the harder problem of extensional waves will be treated fully in a later publication.

EQUATIONS OF POROELASTICITY

For long-wavelength disturbances ($\lambda >> h$, where h is a typical pore size) propagating through a porous medium, we define average values of the (local) displacements in the solid and also in the saturating fluid. The average displacement vector for the solid frame is $\mathbf{u}$ while that for the pore fluid is $\mathbf{u}_f$. The average displacement of the fluid relative to the frame is $\mathbf{w} = \phi(\mathbf{u} - \mathbf{u}_f)$. For small strains, the frame dilatation is

$$e = e_x + e_y + e_z = \nabla \cdot \mathbf{u}, \tag{1}$$

where e_x,e_y,e_z are the Cartesian strain components. Similarly, the average fluid dilatation is

$$e_f = \nabla \cdot \mathbf{u}_f \tag{2}$$

(e_f also includes flow terms as well as dilatation) and the increment of fluid content is defined by

$$\zeta = -\nabla \cdot \mathbf{w} = \phi(e - e_f). \tag{3}$$

With these definitions, Biot (1962) obtains the stress-strain relations in the form

$$\delta\tau_{xx} = He - 2\mu(e_y + e_z) - C\zeta, \tag{4}$$

and similarly (with permutations) for the other compressional components $\delta\tau_{yy}$,$\delta\tau_{zz}$, while

$$\delta\tau_{zx} = \mu\left(\frac{\partial u_x}{\partial z} + \frac{\partial u_z}{\partial x}\right), \tag{5}$$

and again for $\delta\tau_{yz}$,$\delta\tau_{xy}$ for the other shear components. And finally, for the fluid pressure,

$$\delta p_f = M\zeta - Ce. \tag{6}$$

The $\delta\tau_{ij}$ are deviations from equilibrium of average Cartesian stresses in the saturated porous material and δp_f is similarly the isotropic pressure deviation in the pore fluid.

With time dependence of the form $\exp(-i\omega t)$, the coupled wave equations that incorporate (4)-(6) are of the form

$$\begin{aligned} \omega^2(\rho\mathbf{u}+\rho_f\mathbf{w}) &= C\nabla\zeta - (H-\mu)\nabla e - \mu\nabla^2\mathbf{u}, \\ \omega^2(\rho_f\mathbf{u}+q\mathbf{w}) &= M\nabla\zeta - C\nabla e, \end{aligned} \tag{7}$$

where $\rho = \phi\rho_f + (1-\phi)\rho_m$ is the bulk-density of the material and $q = \rho_f\left[\alpha/\beta + iF(\xi)\eta/\kappa\omega\right]$ is the effective density of the fluid in relative motion. The kinematic viscosity of the liquid is η; the permeability of the porous frame is κ; the dynamic viscosity factor is given, for our choice of sign for the frequency dependence, by $F(\xi) = \frac{1}{4}\{\xi T(\xi)/[1+2T(\xi)/i\xi]\}$, where $T(\xi) = \frac{\mathrm{ber}'(\xi)-i\mathrm{bei}'(\xi)}{\mathrm{ber}'(\xi)-i\mathrm{bei}'(\xi)}$ and $\xi = (\omega h^2/\eta)^{\frac{1}{2}}$. The functions ber($\xi$) and bei($\xi$) are the real and imaginary parts of the Kelvin function. The dynamic parameter h is a characteristic length generally associated with and comparable in magnitude to the steady-flow hydraulic radius. The tortuosity $\alpha \geq 1$ is a pure number related to the frame inertia which has been measured by Johnson *et al.* (1982) and has also been estimated theoretically by Berryman (1980a,b).

The coefficients H, C, and M are given by [see Gassmann (1951), Geertsma (1957), Biot and Willis (1957), Geertsma and Smit (1961), and Stoll (1974)]

$$H = K + \frac{4}{3}\mu + (K_m - K)^2/(D-K), \tag{8}$$

$$C = K_m(K_m - K)/(D-K), \tag{9}$$

and

$$M = K_m^2/(D-K), \tag{10}$$

where

$$D = K_m[1+\phi(K_m/K_f - 1)]. \tag{11}$$

Equations (8)-(11) are correct as long as the porous material may be considered homogeneous on the microscopic scale as well as the macroscopic scale.

To decouple the wave equations (7) into Helmholtz equations for the three modes of propagation, we note that the displacements $\mathbf{u}$ and $\mathbf{w}$ can be decomposed as

$$\mathbf{u} = \nabla\Upsilon + \nabla\times\boldsymbol{\beta}, \qquad \mathbf{w} = \nabla\psi + \nabla\times\boldsymbol{\chi}, \tag{12}$$

where Υ, ψ are scalar potentials and $\boldsymbol{\beta}$, $\boldsymbol{\chi}$ are vector potentials. Substituting (12) into (7), we find (7) is satisfied if two pairs of equations are satisfied:

$$(\nabla^2 + k_s^2)\boldsymbol{\beta} = 0, \qquad \boldsymbol{\chi} = -\rho_f\boldsymbol{\beta}/q \tag{13}$$

and

$$(\nabla^2 + k_\pm^2)A_\pm = 0. \tag{14}$$

The wavenumbers in (13) and (14) are defined by

$$k_s^2 = \omega^2(\rho - \rho_f^2/q)/\mu \tag{15}$$

and

$$k_\pm^2 = \tfrac{1}{2}\left\{b + f \mp [(b-f)^2 + 4cd]^{\frac{1}{2}}\right\}, \tag{16}$$

$$\begin{aligned} b = \omega^2(\rho M - \rho_f C)/\Delta,\ c = \omega^2(\rho_f M - qC)/\Delta, \\ d = \omega^2(\rho_f H - \rho C)/\Delta,\ f = \omega^2(qH - \rho_f C)/\Delta, \end{aligned} \tag{17}$$

with $\Delta = MH - C^2$. The linear combination of scalar potentials has been chosen to be $A_\pm = \Gamma_\pm \Upsilon + \psi$, where

$$\Gamma_\pm = d/(k_\pm^2 - b) = (k_\pm^2 - f)/c. \tag{18}$$

With this identification (18) of the coefficients $\Gamma_\pm$, the decoupling is complete.

Equations (13) and (14) are valid for any choice of coordinate system. They may be applied to boundary value problems with arbitrary symmetry. Biot's theory will therefore be applied to porous elastic cylinders in the next section.

EQUATIONS FOR A POROUS CYLINDER

To work most easily in cylindrical geometry, we rewrite the stress-strain relations (4)-(6) in cylindrical coordinates. If z is the coordinate along the cylinder axis while r and θ are the radial and azimuthal coordinates, it is not difficult to show that

$$\delta\tau_{rr} = He - 2\mu(e_\theta + e_z) - C\zeta, \tag{19}$$

$$\delta\tau_{r\theta} = \mu\left(\frac{\partial u_\theta}{\partial r} - \frac{u_\theta}{r} + \frac{1}{r}\frac{\partial u_r}{\partial \theta}\right), \tag{20}$$

$$\delta\tau_{rz} = \mu\left(\frac{\partial u_r}{\partial z} + \frac{\partial u_z}{\partial r}\right), \tag{21}$$

and (6) for δp_f remains unchanged. The stress increments $\delta\tau_{zz}$, $\delta\tau_{\theta\theta}$, and $\delta\tau_{\theta z}$ are not of direct interest in the present application. The dilatations are given by

$$e = e_r + e_\theta + e_z, \tag{22}$$

where

$$e_r = \frac{\partial u_r}{\partial r}, \quad e_\theta = \frac{u_r}{r} + \frac{1}{r}\frac{\partial u_\theta}{\partial \theta}, \quad e_z = \frac{\partial u_z}{\partial z}. \tag{23}$$

We redefine potential $\boldsymbol{\beta}$ in terms of two scalar potentials according to

$$\boldsymbol{\beta} = \hat{\mathbf{z}}\beta_1 + \nabla \times (\hat{\mathbf{z}}\beta_2), \tag{24}$$

where both β_i satisfy

$$(\nabla^2 + k_s^2)\beta_i = 0 \qquad \text{for} \qquad i = 1,2. \tag{25}$$

For the problem of interest here, we will have two distinct regions: The first region is a cylinder centered at the origin, within which solutions of (14) and (25) must be finite at the origin. Results take the form

$$A_\pm = \alpha_\pm J_0(j_\pm) \exp i(k_z z - \omega t), \tag{26}$$
$$\beta_1 = \gamma_s J_0(j_s) \exp i(k_z z - \omega t), \tag{27}$$
$$\beta_2 = (\alpha_s / i k_z) J_0(j_s) \exp i(k_z z - \omega t), \tag{28}$$

where

$$j_\pm = k_{\pm r} r, \qquad j_s = k_{sr} r \tag{29}$$

and

$$k_{\pm r}^2 = k_\pm^2 - k_z^2, \qquad k_{sr}^2 = k_s^2 - k_z^2. \tag{30}$$

J_0 is the zero-order Bessel function of the first kind. The coefficients $\alpha_\pm$, α_s, γ_s, are constants to be determined from the boundary conditions.

The second region is a cylindrical shell around the first region. In this region, the factors $k_\pm$ and k_s take different values from the those in the central region, indicated by $k_\pm^*$ and k_s^* (where $*$ means air-filled, and does *not* ever mean complex conjugate in this paper). Furthermore, two linearly independent solutions of the equations are allowed, *i.e.*, both J_0 and Y_0 (the Bessel function of the second kind, sometimes known as the Neumann function). In the outer shell, we have four coefficients apiece for J_0 and Y_0, all of which must also be determined by the boundary conditions.

Noting that

$$\Upsilon = (A_+ - A_-)/(\Gamma_+ - \Gamma_-),$$
$$\psi = (A_+\Gamma_- - A_-\Gamma_+)/(\Gamma_- - \Gamma_+) \tag{31}$$

from the definitions of $A_\pm$, and substituting (26)-(28) and (31) into (12), and the result into (6) and (19)-(21), we finally obtain

$$\delta\tau_{r\theta} = m_{11}\gamma_s \equiv -\mu k_{sr}^2 J_2(j_s)\gamma_s, \tag{32}$$
$$\delta\tau_{rr} = a_{11}\alpha_+ + a_{12}\alpha_- + a_{13}\alpha_s, \tag{33}$$
$$-\delta p_f = a_{21}\alpha_+ + a_{22}\alpha_- + a_{23}\alpha_s, \tag{34}$$
$$\delta\tau_{rz} = a_{31}\alpha_+ + a_{32}\alpha_- + a_{33}\alpha_s, \tag{35}$$

where

$$(\Gamma_+ - \Gamma_-)a_{11} = \left[(C\Gamma_- - H)k_+^2 + 2\mu k_z^2\right] J_0(j_+) + 2\mu k_{+r} J_1(j_+)/r, \tag{36}$$

$$(\Gamma_+ - \Gamma_-)a_{12} = -2\mu k_{-r}^2 J_1(j_-)/j_- + \left[(H - C\Gamma_+)k_-^2 - 2\mu k_z^2\right] J_0(j_-), \tag{37}$$

$$a_{13} = 2\mu k_{sr}^2 J_2(j_s), \tag{38}$$

$$(\Gamma_+ - \Gamma_-)a_{21} = (M\Gamma_- - C)k_+^2 J_0(j_+), \tag{39}$$

$$(\Gamma_+ - \Gamma_-)a_{22} = (C - M\Gamma_+)k_-^2 J_0(j_-), \tag{40}$$

$$(\Gamma_+ - \Gamma_-)a_{31} = -2i\mu k_z k_{+r} J_1(j_+), \tag{41}$$

$$(\Gamma_+ - \Gamma_-)a_{32} = 2i\mu k_z k_{-r} J_1(j_-), \tag{42}$$

$$ik_z a_{33} = -\mu(k_s^2 - 2k_z^2)k_{sr} J_1(j_s), \tag{43}$$

and $a_{23} = 0$. There is an implicit factor of $\exp i(k_z z - \omega t)$ on the right-hand side of (32)-(35).

Berryman (1983) has shown that a_{11}, a_{13}, a_{31}, and a_{33} reduce in the limit $\phi \to 0$ to the corresponding results for isotropic elastic cylinders by Pochhammer (1876), Chree (1886, 1889), Love (1941), and Bancroft (1941), as they should.

BOUNDARY CONDITIONS

Appropriate boundary conditions for use with Biot's equations have been considered by Deresiewicz and Skalak (1963), Berryman and Thigpen (1985), and Pride and Haartsen (1996) and we make use of these results here.

At the external surface $r = R_2$ where the outer porous material contacts the surrounding air, it is appropriate to use the free surface conditions

$$-\delta p_f = 0,\ \delta\tau_{rr} = 0,\ \delta\tau_{r\theta} = 0,\ \delta\tau_{rz} = 0, \tag{44}$$

for the deviations from static equilibrium. If the cylinder is sealed on $r = R_2$, then the first of these needs to be replaced by $w_r = 0$.

The internal interface at $r = R_1$ needs more precise definition. We assume that all the meniscii that are separating the inner fluid from the outer fluid are contained within a thin layer

(shell) of thickness δh (a few grain sizes in width) straddling the surface $r = R_1$. All fluid that enters this interface layer goes into stretching the meniscii since as Pride and Flekkoy (1999) have shown, it is reasonable to assume that the contact lines of the meniscii remain pinned under seismic stressing. The locally incompressible flow conserves fluid volume so that the rate at which the inner fluid enters the interface layer is equal to the rate at which the outer fluid leaves the layer thus requiring

$$\dot{w}_r(r = R_1 + \delta h/2) = \dot{w}_r^*(r = R_1 - \delta h/2). \tag{45}$$

This and the following conditions are to be understood in the limit where $\delta h/R_1 \to 0$. It is also straightforward to obtain the standard results

$$\tau_{rr} = \tau_{rr}^*, \;\; \tau_{r\theta} = \tau_{r\theta}^*, \;\; \tau_{rz} = \tau_{rz}^*, \tag{46}$$

and

$$\dot{u}_r = \dot{u}_r^*, \;\; \dot{u}_\theta = \dot{u}_\theta^*, \;\; \dot{u}_z = \dot{u}_z^*. \tag{47}$$

The final condition to establish on $r = R_1$ is that involving the fluid pressure.

The rate at which energy fluxes radially through the porous material is given by $\tau_{ri}\dot{u}_i - p_f\dot{w}_r$ with implicit summation over the index i. The difference in the rate at which energy is entering and leaving the interface layer is due to work performed in stretching the meniscii. Each meniscus has an initial mean curvature H_o that is determined by the initial fluid pressures (those that hold before the wave arrives) as $p_{f0} - p_{f0}^* = \sigma H_o$ where σ is the surface tension. As the wave passes, the ratio between the actual mean curvature H and H_o is a small quantity on the order of the capillary number $\epsilon = \eta|\dot{w}_r|/\sigma$ [see Pride and Flekkoy (1999)] where $|\dot{w}_r|$ is some estimate of the induced Darcy flow and that goes as wave strain times wave velocity ($|\dot{w}_r| < 10^{-3}$ m/s). Since $\sigma > 10^{-2}$ Pa·m for air-water interfaces, we have $\epsilon < 10^{-4}$, which can be considered negligible. By integrating the energy flux rate over a Gaussian shell that straddles $r = R_1$, it is straightforward to obtain

$$\begin{aligned} &[\tau_{ri}\dot{u}_i - (p_{f0} + \delta p_f)\dot{w}_r] - \\ &[\tau_{ri}^*\dot{u}_i^* - (p_{f0}^* + \delta p_f^*)\dot{w}_r^*] = \sigma H_o \dot{w}_r[1 + O(\epsilon)]. \end{aligned} \tag{48}$$

Thus, since all components here except fluid pressure are continuous, we find that, when ϵ is small compared to unity,

$$\delta p_f = \delta p_f^*. \tag{49}$$

In other words, to the extent that the capillary number can be considered small (always the case for linear wave problems), the wave-induced increments in fluid pressure are continuous at $r = R_1$.

To apply the boundary conditions (45) and (49), we need in addition to (34) the result

$$w_r = a_{41}\alpha_+ + a_{42}\alpha_- + a_{43}\alpha_s, \tag{50}$$

where

$$(\Gamma_+ - \Gamma_-)a_{41} = k_{+r} J_1(j_+)\Gamma_-, \tag{51}$$
$$(\Gamma_+ - \Gamma_-)a_{42} = -k_{-r} J_1(j_-)\Gamma_+, \tag{52}$$
$$a_{43} = k_{sr} J_1(j_s)\rho_f/q. \tag{53}$$

The remaining stress conditions (46) are determined by (33) and (35).

To apply the boundary conditions (47), we need the explicit expressions for the displacement which follow from (12). The results are of the form

$$u_r = a_{51}\alpha_+ + a_{52}\alpha_- + a_{53}\alpha_s, \tag{54}$$

where

$$(\Gamma_+ - \Gamma_-)a_{51} = -k_{+r} J_1(j_+), \tag{55}$$
$$(\Gamma_+ - \Gamma_-)a_{52} = k_{-r} J_1(j_-), \tag{56}$$
$$a_{53} = k_{sr} J_1(j_s), \tag{57}$$

and

$$u_z = a_{61}\alpha_+ + a_{62}\alpha_- + a_{63}\alpha_s, \tag{58}$$

where $a_{61} = a_{62} = 0$, and

$$a_{63} = k_{sr}^2 J_0(j_s)/ik_z. \tag{59}$$

Both (54) and (58) are needed for extensional waves, while the remaining component,

$$u_\theta = m_{21}\gamma_s \equiv k_{sr} J_1(j_s)\gamma_s, \tag{60}$$

is needed only for torsional waves. As before, there is an implicit factor of $\exp i(k_z z - \omega t)$ on the right-hand side of (51)-(53), (55)-(57), and (59).

It follows from (32)-(35), (50), and (60) that γ_s (for the inner cylinder) and the corresponding coefficients for the cylindrical shell are all completely independent of the other mode coefficients and, therefore, relevant to the study of torsional waves, but not for extensional waves. Pertinent equations for the torsional wave dispersion relation are continuity of the angular displacement, u_θ, and stress, $\tau_{r\theta}$, at the internal interface, and vanishing of the stress, $\tau_{r\theta}$, at the external surface.

The final set of equations for the extensional wave dispersion relation involves nine equations with nine unknowns. The nine unknowns are: α_+, α_-, α_s (coefficients of J_0 in the central cylinder), plus three α^*'s (coefficients of J_0) and three η^*'s (coefficients of Y_0) for region of the cylindrical shell. The nine equations are: the continuity of radial and one tangential stress as well as radial and one tangential displacement at the interfacial boundary (totaling four conditions), continuity of fluid pressure and normal fluid increments across the same boundary (two conditions), and finally the vanishing of the external fluid pressure, radial and one tangential stress at the free surface (three conditions). The extensional wave dispersion relation is then determined as in Berryman (1983) by those conditions on the wavenumber k_z that result in vanishing of the determinant of the coefficients of this 9×9 complex matrix.

ELEMENTARY TORSIONAL MODES

The torsional mode of cylinder oscillation (which is trivial for a simple cylinder, porous or not) is determined here by a 3×3 system, of which 8 elements are in general nonzero. This system is therefore similar in size and difficulty to the cases studied earlier by Berryman (1983) for extensional waves in a simple fully saturated poroelastic cylinder. On the other hand, for extensional waves, the matrix determining the extensional wave dispersion relation for patchy saturation has 81 elements, of which 69 will in general be nonzero. This problem requires sufficiently different treatment from that for the torsional case that we set it aside to be studied fully in a future publication.

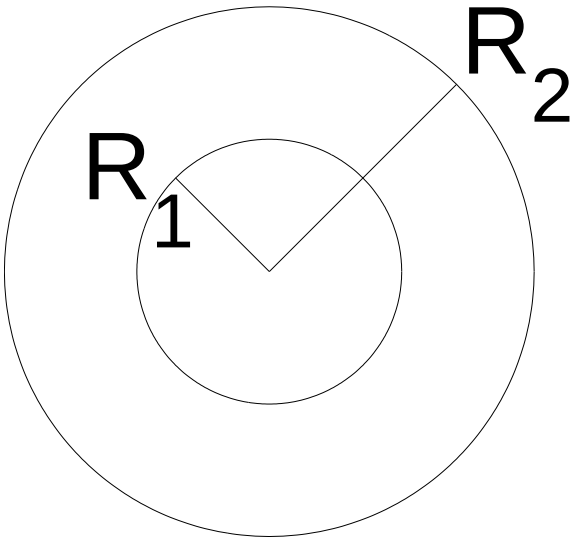

Figure 1: Cross-section of a circular cylinder, where $R_1 = S^{\frac{1}{2}} R_2$ is determined by the liquid saturation level S. jim2-concentric [NR]

We assume that the cylinder has liquid saturation level $S = (R_1/R_2)^2$, where R_2 is the radius of the cylinder and $r = R_1$ is the location of the liquid-gas interface (see Fig. 1). The dispersion relation for torsional waves is then given by

$$\begin{vmatrix} m_{11}^*(R_2) & n_{11}^*(R_2) & 0 \\ -m_{11}^*(R_1) & -n_{11}^*(R_1) & m_{11}(R_1) \\ -m_{21}^*(R_1) & -n_{21}^*(R_1) & m_{21}(R_1) \end{vmatrix} = 0, \tag{61}$$

where m_{11} and m_{21} are given by (32) and (60). The coefficients m_{11}^* and m_{12}^* have the same functional forms as m_{11} and m_{21}, but the constants are those for the shell, rather than the inner cylinder. Similarly, n_{11}^* and n_{12}^* are just the same as m_{11}^* and m_{12}^* except that J_0 and J_1 are replaced everywhere by Y_0 and Y_1, respectively.

Now we notice immediately that there could be two elementary solutions of (61), one with $m_{11}^*(R_2) = n_{11}^*(R_2) = 0$ (exterior condition) and another with $m_{11}(R_1) = m_{21}(R_1) = 0$ (interior condition). First, the interior condition is satisfied, for example, when $k_{sr} = 0$ or, equivalently, when $k_z^2 = k_s^2$. This corresponds to a torsional mode of propagation having wave speed and attenuation determined exactly by the bulk shear wave in the interior region, but the interior region is not moving since $k_{sr} = 0$ also implies that $u_\theta = 0$ from (60). Thus, the interior

condition results in the drained outer shell twisting around a stationary inner liquid-saturated cylinder. Second, the exterior condition is similarly satisfied when $k_{sr}^* = 0$ or, equivalently, when $k_z^2 = (k_s^*)^2$. This condition looks at first glance as if it might be spurious because $k_{sr}^* = 0$ suggests that u_θ at the exterior boundary might vanish identically, and then this would correspond to a trivial solution of the equations. However, looking closer, this is not the case, because at the external boundary

$$u_\theta = k_{sr}^* \left[J_1(j_s^*)\gamma_s^* + Y_1(j_s^*)\epsilon_s^* \right], \tag{62}$$

so as $k_{sr}^* \to 0$, the first term on the right hand side of (62) does vanish, both because $k_{sr}^* \to 0$ and also because $J_1(j_s^*) \to 0$. But the second term does not vanish in this limit because $|Y_1(j_s^*)| \to 2/\pi k_{sr}^* R_2 \to \infty$ as $k_{sr}^* \to 0$, and the product gives the finite result: $2/\pi R_2$. So this condition is not spurious, and corresponds to a torsional wave propagating with the speed and attenuation of the bulk shear wave speed in the drained shell material.

Can both of these elementary modes be excited? If we assume for the moment that Gassmann's equations (1951) [also see Berryman (1999)] apply to the sample, then $\mu^* = \mu$ and the only changes in shear wave velocity in the two regions are those induced by the changes in mass. In this situation, the wave speed in the air/gas saturated region will be faster than that in the water/liquid saturated region, since liquid is more dense than gas. Thus, the real part of k_s^* is smaller than that of k_s, and while the condition $(k_{sr}^*)^2 = 0$ implies that the real part of k_{sr}^2 is positive, the condition $k_{sr}^2 = 0$ implies that the real part of $(k_{sr}^*)^2$ is negative. Therefore, assuming (as we generally do here) that the attenuation in the system is relatively small, the condition $k_z = k_s^*$ leads to a propagating wave, while $k_z = k_s$ leads to a strongly evanescent wave. Note that, if Gassmann's results do not apply to the system (say at ultrasonic frequencies), then the results of the preceeding paragraph may need to be reconsidered. In particular, if the shear modulus changes rapidly with the introduction of liquid saturant, it is possible that the shear wave speed for a liquid saturated porous material may be higher than that for the gas saturated case. In this situation, all the inequalities of the preceding paragraph would be reversed, and then the condition $k_z = k_s$ leads to a propagating wave, while $k_z = k_s^*$ leads to a strongly evanescent wave.

Our conclusion then is that both modes can indeed be excited, but probably not simultaneously in the same system in the same frequency band. In a highly dispersive porous system and with broadband acoustic signal input, it could happen that both modes are propagating simultaneously in time, but in distinct/disjoint frequency bands.

HIGHER ORDER TORSIONAL MODES

For fully saturated porous cylinders, the factor that determines the torsional modes of propagation is $m_{11}(r)$ in (32). The critical factor here is the Bessel function $J_2(j_s)$ and, specifically, the whereabouts of its zeroes. One source of this information, to five figure accuracy, is the reference of Abramowitz and Stegun (1965), which provides not only the location of the zeroes $j_{2,n}$, but also the values of the corresponding derivatives $J_2'(j_{2,n})$. Having these derivatives is useful for improving the accuracy of the zeroes with a Newton-Raphson iterative method,

based on $j_{2,n} = j_{2,n}^{old} - J_2(j_{2,n}^{old})/J_2'(j_{2,n}^{old})$. This approach gives a very rapid improvement to the values of the $j_{2,n}$'s within 2 to 3 iterations. The results to order $n = 3$ are shown in TABLE 1.

TABLE 1. The zeroes $j_{2,n}$ of $J_2(z)$ as a function of the order n of appearance along the real axis.

Order n	$j_{2,n}$
0	0.00000000000000
1	5.13562230184068
2	8.41724414039987
3	11.61984117214906

Having already understood the zeroth order contributions to the dispersion relation (61) due to zeroes of k_{sr} and k_{sr}^*, we are now free to consider that neither of these factors vanishes for the higher order modes. This assumption permits us to factor these wavenumbers in or out of the determinant whenever it is convenient to do so. In particular, we note that the first two columns of (61) would have a common factor of $\mu^*(k_{sr}^*)^2$ (which could then be safely eliminated) if we first multiply the bottom row by a factor of $\mu^* k_{sr}^*$. Having made these simplifications, we find

$$\begin{vmatrix} J_2(k_{sr}^* R_2) & Y_2(k_{sr}^* R_2) & 0 \\ J_2(k_{sr}^* R_1) & Y_2(k_{sr}^* R_1) & \mu k_{sr} J_2(k_{sr} R_1) \\ J_1(k_{sr}^* R_1) & Y_1(k_{sr}^* R_1) & \mu^* k_{sr}^* J_1(k_{sr} R_1) \end{vmatrix} = 0, \tag{63}$$

after also eliminating a common factor of -1 from the top row, and $-k_{sr}$ from the third column.

Expanding the determinant along the third column, we have

$$\begin{aligned} 0 = {} & \mu^* k_{sr}^* J_1(k_{sr} R_1) \begin{vmatrix} J_2(k_{sr}^* R_2) & Y_2(k_{sr}^* R_2) \\ J_2(k_{sr}^* R_1) & Y_2(k_{sr}^* R_1) \end{vmatrix} \\ & - \mu k_{sr} J_2(k_{sr} R_1) \begin{vmatrix} J_2(k_{sr}^* R_2) & Y_2(k_{sr}^* R_2) \\ J_1(k_{sr}^* R_1) & Y_1(k_{sr}^* R_1) \end{vmatrix}. \end{aligned} \tag{64}$$

Some elementary consequences of this equation are: (a) As $R_1 \to 0$ so there is no liquid left in the system, $J_1(k_{sr} R_1)$ and $J_2(k_{sr} R_1) \to 0$ like R_1, while $Y_1(k_{sr}^* R_1)$ and $Y_2(k_{sr}^* R_1) \to \infty$ like $1/R_1$. So the dispersion relation is always satisfied in the limit when $J_2(k_{sr}^* R_2) = 0$, which is exactly the condition for the fully dry cylinder as expected. (b) If $R_1 \to R_2$, then the first determinant vanishes identically. The second determinant does not vanish in general since it approaches the Wronskian $J_2 Y_1 - J_1 Y_2 = 2/\pi k_{sr}^* R_2$, so the condition becomes $k_{sr} J_2(k_{sr} R_1) = 0$, again as expected. (c) The special case of $k_{sr} \to 0$ does not affect these conclusions, as both $J_1(k_{sr} R_1)$ and $J_2(k_{sr} R_1) \to 0$ in this limit, as they should. (d) The only case that is missing

from (64) is the one for $k^*_{sr} \to 0$. But this multiple zero of the original dispersion relation (61) was eliminated when we removed two factors of $(k^*_{sr})^2$ from the first and second column in the first step of our simplification of the dispersion relation – a step which is always legitimate except when $k^*_{sr} \equiv 0$.

We conclude that, with the one trivial exception just noted, these simplifications have kept the basic nature of the dispersion relation intact.

Lower frequency results

At lower frequencies in the range $f < 1kHz$, we may typically expect that Gassmann's results hold for the poroelastic medium, where $\mu^* \equiv \mu$. Also, to a very good approximation $k^*_s \simeq k_s$, where the only deviations from equality are those due to the differences in the densities of liquid and gas constituents. So deviations from this approxiation are most substantial when the porosity is high. From (63), we see that if the the products μk_{sr} and $\mu^* k^*_{sr}$ are equal, then these factors can be removed from the third column of the determinant. Then, the resulting third column can be subtracted from the first column, and the result can be expanded along the first column to give:

$$\frac{2\,J_2(k_{sr}\,R_2)}{\pi\,k_{sr}\,R_1} = 0, \tag{65}$$

having again used the fact that $J_2(z)Y_1(z) - J_1(z)Y_2(z) = 2/\pi z$. So the important zeroes in this case are again those of J_2, some of which are already displayed in TABLE 1.

Ignoring the imaginary part of k, which is usually quite small in the limit, we have the analytical result that

$$v_z^{(n)} = \frac{v_s}{[1 - (j_{2,n}\,v_s/\omega R_2)^2]^{1/2}}. \tag{66}$$

Thus, at the higher frequencies, this velocity approaches that of the shear wave as expected. When the lower frequencies are approached, there is an obvious cutoff frequency, $f_c^n = j_{2,n}\,v_s/2\pi\,R_2$, below which these torsional modes do not propagate for $n \geq 1$. Since this low frequency cutoff may often be in conflict with the assumption under consideration here (*i.e.*, frequencies low enough that Gassmann's equation is satisfied), we expect generally that very few of the higher order modes can be excited in this limit. The main result is therefore that $v_z = v_z^0 = v_s$ is the velocity that will be observed in laboratory experiments in this frequency domain, with only very few exceptions.

We will not consider this rather special case any further in this paper.

Higher frequency results

The more interesting case is that for higher frequencies, in which case it is now understood (Berryman *et al.*, 2000, 2002; Berryman and Wang, 2001) that the simple Biot-Gassmann theory is actually inadequate because there can be dependence of μ on liquid saturant properties at high frequencies, such as $f > 1kHz$. The precise frequency at which this becomes

important is material dependent, but it is generally observed that for ultrasonic frequencies $f > 20kHz$ some deviations from Biot-Gassmann predictions are normally found. So it is in this regime that the distinctions between air-filled and water-filled pores become important for the torsional motion of a cylinder.

Case: $\mu^* = \mu$

Even if there is no difference between μ^* and μ, there can still be significant differences between k_s^* and k_s due to the differences in the fluid viscosities and densities of liquid and gas constituents. So we will treat this case next.

For Massillon sandstone, Murphy (1982, 1984) measured extensional and shear wave velocities at $f = 560$ Hz over a range of partial saturations produced using the drainage method. Relevant properties of this sandstone are listed in TABLE 2.

TABLE 2. Properties of Massillon sandstone used in Murphy's experiments (Murphy, 1982; 1984) and Spirit River sandstone in Knight and Nolen-Hoeksema's experiments (Knight and Nolen-Hoeksema, 1990).

Property	Massillon	Spirit River
Porosity (%)	23.0	5.2
Permeability (mD)	7.37×10^2	1.0×10^{-3}
Grain size (μm)	150–200	125–150

Case: $\mu^* \leq \mu$

The presence of liquid in the pores may alter the mechanical behavior of rocks under shear deformations in at least two quite distinct ways: (a) It is often observed that a very small amount of some liquids can cause chemical interactions that tend to soften the binding material present among the grains of such a system. When this happens, the shear modulus is usually observed to decrease. (See for example FIG. 3 for Sierra White granite.) So this situation implies that $\mu^* \geq \mu$, contrary to Gassmann's results. Although this situation is well-known in practice, we will ignore it in our modeling efforts. Our justification for this will be that the medium we are calling "dry" should in fact be termed "drained" in the sense that it has been wetted previously and therefore has these chemical softening effects already factored into the modulus μ^*. In any case, our goal is not to fit data for specific rocks, but rather to understand general trends. (b) The other situation that can also occur in practice – particularly at higher frequencies – is that the liquid saturating the porous material can have a nonnegligible mechanical effect (Berryman and Wang, 2001) that tends to strengthen the medium under shear loading so that $\mu \geq \mu^*$. If this strengthening effect is great enough (and there are experimental results (see

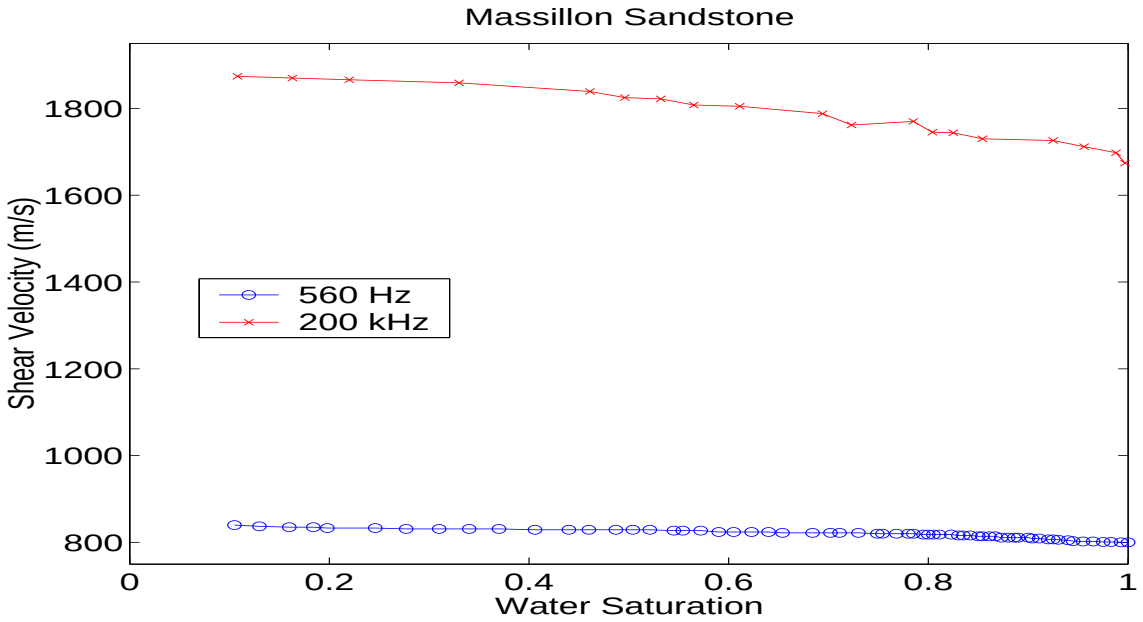

Figure 2: Shear wave velocities as a function of water saturation for drainage experiments of Murphy (1982,1984). jim2-massillon_vs [NR]

FIG. 4) that confirm this does happen in practice (Berryman *et al.*, 2002), then it is possible the density effect is more than counterbalanced by the enhanced shear modulus effect with the result that the speed of shear wave propagation in the liquid saturated medium is greater than that in the air saturated case. Depending on details of the liquid distribution in the pores, either of these cases can be included in the analysis that we now pursue in this subsection.

For Massillon sandstone, Murphy (1982,1984) also measured extensional and shear wave velocities at $f = 200$ kHz over a range of partial saturations produced using the drainage method. Relevant properties of this sandstone were listed before in TABLE 2.

SOLVING THE DISPERSION RELATION

Solving the full complex dispersion relation is somewhat tedious, and we will not try to explain this in detail here. Instead we will show results for two cases: first the Massillon sandstone (at 560 Hz) and then the Sierra White granite (at about 200 kHz). We might expect based just on the frequencies that the sandstone behavior will be close to that predicted by Gassmann, while that of the granite may differ from Gassmann.

An important observation concerning how to proceed with the analysis follows from the fact that we are seeking a curve in the complex plane, points along the curve depending on the level of saturation S. We know (at least in principle) the locations of the end points of this curve since they are exactly the points for full liquid saturation and full gas saturation. If we assume that the attenuation is relatively small so the wavenumbers k_s and k_s^* have small

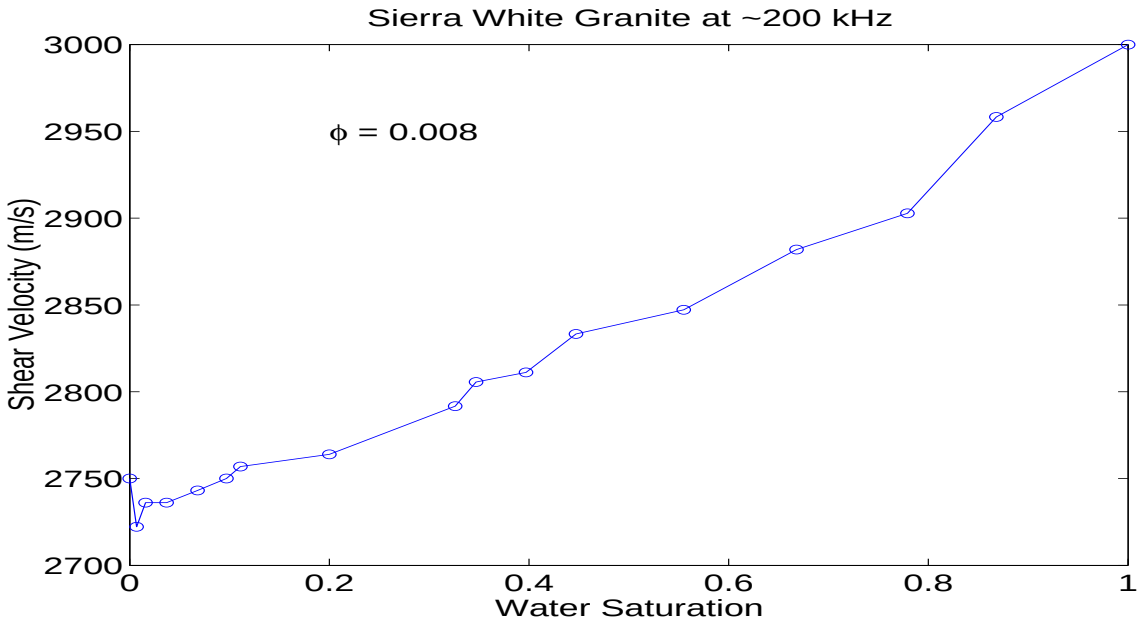

Figure 3: Shear wave velocities as a function of water saturation for drainage experiments of Murphy (1982) in Sierra White granite. jim2-swg200vs [NR]

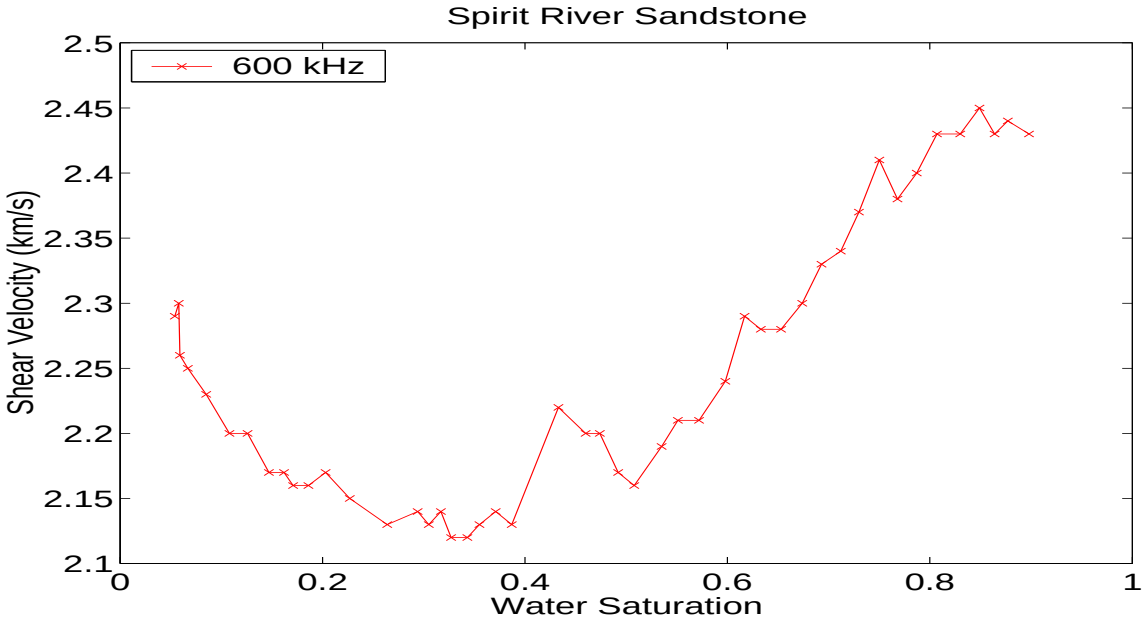

Figure 4: Shear wave velocities as a function of water saturation for drainage experiments of Knight and Nolen-Hoeksema (1990) in Spirit River sandstone. jim2-knight_vs [NR]

imaginary parts, then to a reasonable approximation it is the case that the curve of interest lies close to the real axis in the complex k_z^2-plane. If the imaginary parts exactly vanish, the curve reduces to a straight line on the real axis in this plane. These observations suggest that it might be helpful to trace rays in the complex plane radiating out from the origin, and in particular a ray (*i.e.*, a straight line) passing through the origin and also through the point corresponding to whichever point, k_s^2 or $(k_s^*)^2$, happens to lie closest to the origin should provide a good starting point for the analysis. Another alternative is to consider the straight line that connects these two points directly, even though it would generally not also be a ray through the origin (except for the special case when there is no attenuation). Both of these alternatives have been tried.

The first alternative, a ray through the origin and then passing through the closest point k_s^2 or $(k_s^*)^2$, has the very important characteristic that the values of the dispersion function become purely imaginary in the shadow of the starting point of the curve. This fact provides a great simplification because we need the dispersion function to vanish identically – both in real and imaginary parts, and this shadow region has the nice characteristic that the real part is automatically zero. So the only remaining issue is to check where the imaginary part vanishes. This procedure is much easier to implement and to understand intuitively than trying to find the complex zeroes using something like a Newton method, which could also be implemented for this problem.

The second alternative is not as rigorous as the first, but for the case of small attenuation gives very similar results and is especially easy to implement. In this case we need only consider the line connecting the two points k_s^2 and $(k_s^*)^2$ in the complex plane. It turns out that in the two cases considered here, the real part of the dispersion function is again either zero or very small, so that it makes sense to treat this approach as an approximation to the first one in that we need only seek the points where the imaginary part vanishes. This procedure is very intuitive and examples are shown in FIGS. 5 through 8.

Massillon sandstone

For Massillon, we have the Gassmann-like situation in which the shear wave speed for the drained case is smaller than that for the fully saturated case and therefore $Re(k_s^*) < Re(k_s)$. FIG. 5 shows how the imaginary parts of the dispersion function change in this case as the real part of k_z^2 varies from $Re((k_s^*)^2)$ to $Re(k_s^2)$ (*i.e.*, from air saturated to water saturated). FIG. 5 shows four of these curves ($S = 0.2$ to 0.8). FIG. 6 was generated by completing the procedure for 19 equally spaced points in saturation S. FIG. 6 shows furthermore that the curve obtained actually fits the data for Massillon better than Gassmann does (the straight line between the end points). This is a bit of a surprise as virtually everyone (including the present authors) have often considered these data to be the best known proof of the accuracy of Gassmann's equations for partial saturation problems.

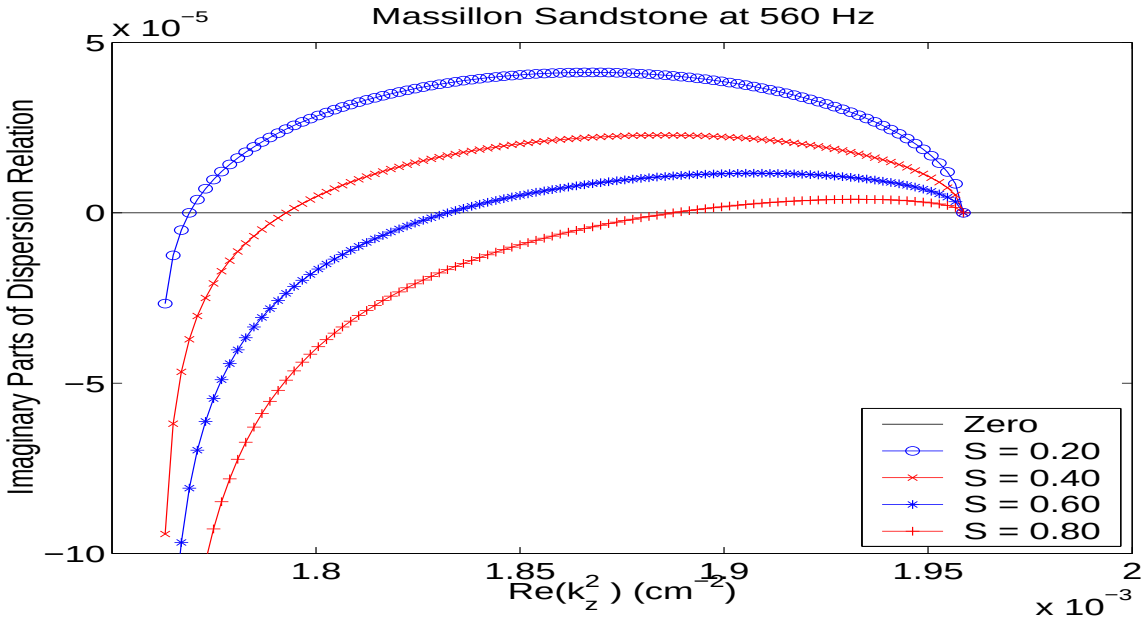

Figure 5: Showing how the imaginary parts of the dispersion relation for Massillon sandstone change in the complex k_z^2 plane as k_z varies from k_{sa} to k_{sw}. The real part of the dispersion relation is either zero or very close to zero along this line and therefore the desired points are those where the imaginary part crosses the zero line. jim2-reimdisp_mss560_20406080_ray3 [NR]

Sierra White granite

For Sierra White, we have the non-Gassmann-like situation in which the shear wave speed for the drained case is larger than that for the fully saturated case and therefore $Re(k_s^*) > Re(k_s)$. FIG. 7 shows how the imaginary parts of the dispersion function change in this case as the real part of k_z^2 varies from $Re(k_s^2)$ to $Re((k_s^*)^2)$ (*i.e.*, from water saturated to air saturated). FIG. 7 shows four of these curves ($S = 0.2$ to 0.8). FIG. 8 was generated by completing the procedure for 19 equally spaced points in saturation S. FIG. 8 shows furthermore that both data and the curve obtained here differ substantially from the simple straightline average that might have been anticipated and, furthermore, that the curve does in fact move in the right direction to agree with the data. This is also a pleasant surprise as it was certainly not known by us what to expect in this situation since our common understanding of poroelasticity does not extend to this rather difficult set of partial saturation problems.

General behavior of the curves

Since the curves obtained in FIGS. 6 and 8 are very well-behaved, it seemed like a good idea to check for simple dependencies on the saturation parameter S. Both curves look like they might be quadratic in S. This hypothesis is tested in FIGS. 9 and 10. We find that the quadratic dependence is essentially exact to graphical accuracy for Massillon sandstone, and it is close

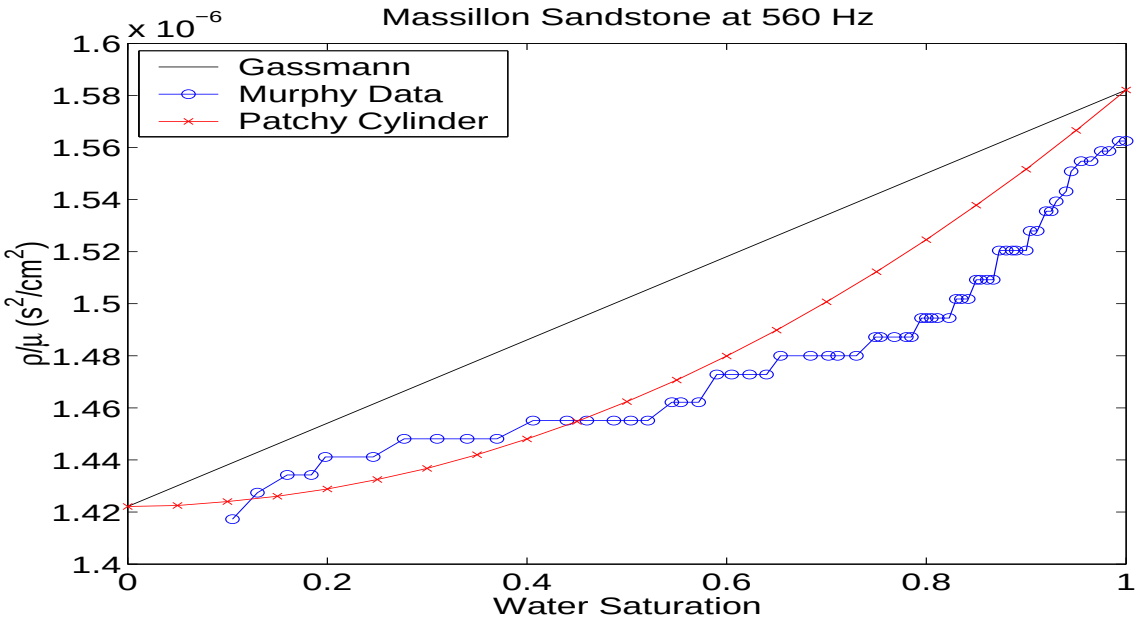

Figure 6: Comparison between the points that solve the dispersion relation for the patchy cylinder, plotted as $\rho/\mu = 1/v_s^2$ versus water saturation S, for Massillon sandstone at 560 Hz. Data are from Murphy. The Gassmann curve is computed assuming that the shear modulus μ is constant and that the only quantity chaning is therefore the density ρ. jim2-mss_rhovmu [NR]

but not exact for the Sierra White granite. We have not yet tried to analyze this behavior and will therefore not attempt an explanation of it at this time.

SUMMARY

Biot slow-wave effects in layered materials have been studied previously by Pride *et al.* (2002) and many others found in their references. The present work is motivated by the desire to understand how fluids interacting with common poroelastic systems may create viscous attenuation in partially saturated (and especially in patchy saturated) cylinders. These effects can then be observed in the attenuation of extensional and torsional waves. There are large quantities of such data already available, and one thrust of our future work will be to reanalyze these data in light of the methods developed here. We have concentrated on analysis of the wave velocities here, as this is clearly the first essential step in the overall analysis of these problems.

ACKNOWLEDGMENTS

We thank Bill Murphy and Rosemary Knight for providing access to their unpublished data files. We thank Brad Artman for helpful comments on the manuscript.

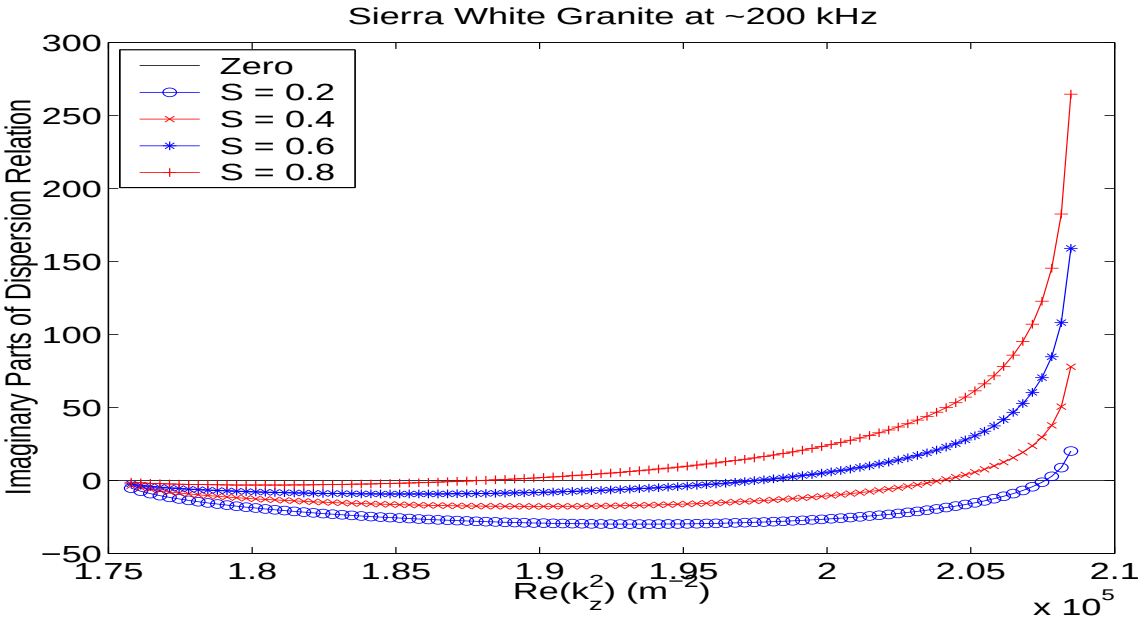

Figure 7: Showing how the imaginary parts of the dispersion relation for Sierra white granite change in the complex k_z^2 plane as k_z varies from k_{sa} to k_{sw}. The real part of the dispersion relation is either zero or very close to zero along this line and therefore the desired points are those where the imaginary part crosses the zero line. jim2-swgdisp_20406080 [NR]

REFERENCES

Abramowitz, M., and Stegun, I. A., 1965, *Handbook of Mathematical Functions*, Dover, New York, Chapter 9.

Avellaneda, M., 1987, Iterated homogenization, differential effective medium theory and applications: *Commun. Pure Appl. Math* **40**, 527–554.

Bancroft, D., 1941, The velocity of longitudinal waves in cylindrical bars: *Phys. Rev.*, **59**, 588–593.

Berge, P. A., Bonner, B. P., and Berryman, J. G., 1995, Ultrasonic velocity-porosity relationships for sandstone analogs made from fused glass beads: *Geophysics* **60**, 108–119.

Berryman, J. G., 1980a, Long-wavelength propagation in composite elastic media. I. Spherical inclusions: *J. Acoust. Soc. Am.* **68**, 1809–1819.

Berryman, J. G., 1980b, Long-wavelength propagation in composite elastic media II. Ellipsoidal inclusions: *J. Acoust. Soc. Am.* **68**, 1820–1831.

Berryman, J. G., 1983, Dispersion of extensional waves in fluid-saturated porous cylinders at ultrasonic frequencies: *J. Acoust. Soc. Am.*, **74**, 1805–1812.

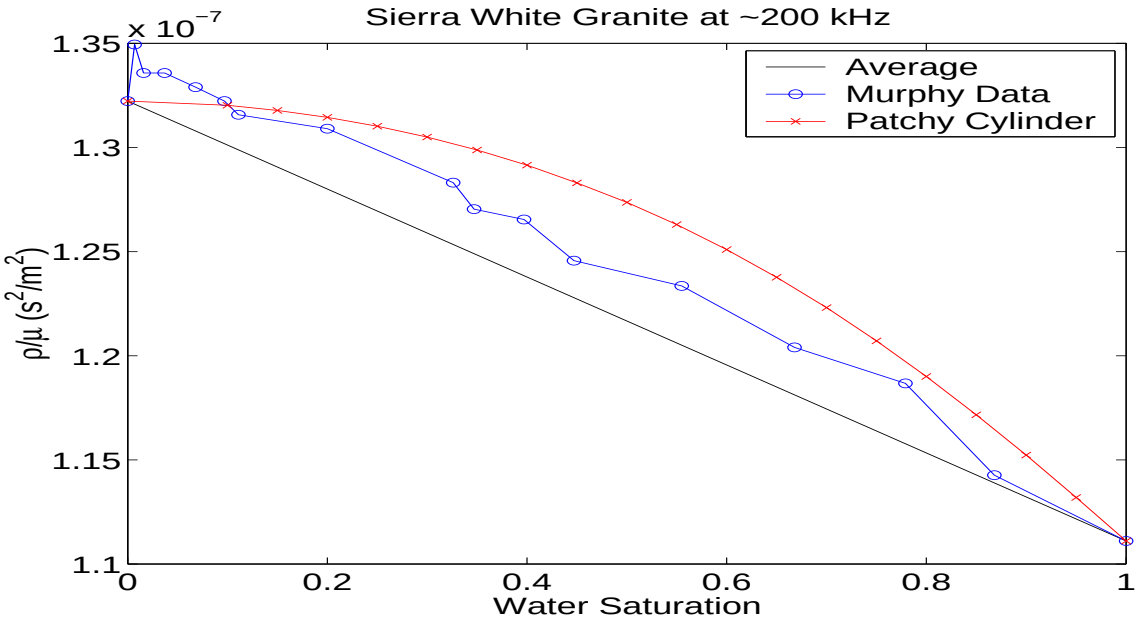

Figure 8: Comparison between the points that solve the dispersion relation for the patchy cylinder, plotted as $\rho/\mu = 1/v_s^2$ versus water saturation S, for Sierra White granite at 200 kHz. Data are from Murphy. For Sierra White, Gassmann's equation clearly does not apply since the shear modulus μ must have increased with water saturation. Data and patchy calculation results are therefore compared to the saturation weighted mean of $1/v_s^2$ in analogy to the Gassmann result. jim2-swg_rhovmu [NR]

Berryman, J. G., 1992, Single-scattering approximations for coefficients in Biot's equations of poroelasticity: *J. Acoust. Soc. Am.* **91**, 551–571.

Berryman, J. G., 1999, Origin of Gassmann's equations: *Geophysics* **64**, 1627–1629.

Berryman, J. G., Berge, P. A., and Bonner, B. P., 2000, Transformation of seismic velocity data to extract porosity and saturation values for rocks: *J. Acoust. Soc. Am.* **107**, 3018–3027.

Berryman, J. G., Berge, P. A., and Bonner, B. P., 2002a, Estimating rock porosity and fluid saturation using only seismic velocities: *Geophysics* **67**, 391–404.

Berryman, J. G., Pride, S. R., and Wang, H. F., 2002b, A differential scheme for elastic properties of rocks with dry or saturated cracks: *Geophys. J. Int.*, accepted for publication in 2002.

Berryman, J. G., Thigpen, L., and Chin, R. C. Y., 1988, Bulk elastic wave propagation in partially saturated porous solids: *J. Acoust. Soc. Am.* **84**, 360–373.

Berryman, J. G, and Wang, H. F., 2001, Dispersion in poroelastic systems: *Phys. Rev. E* **64**, 011303-1–011303-16.

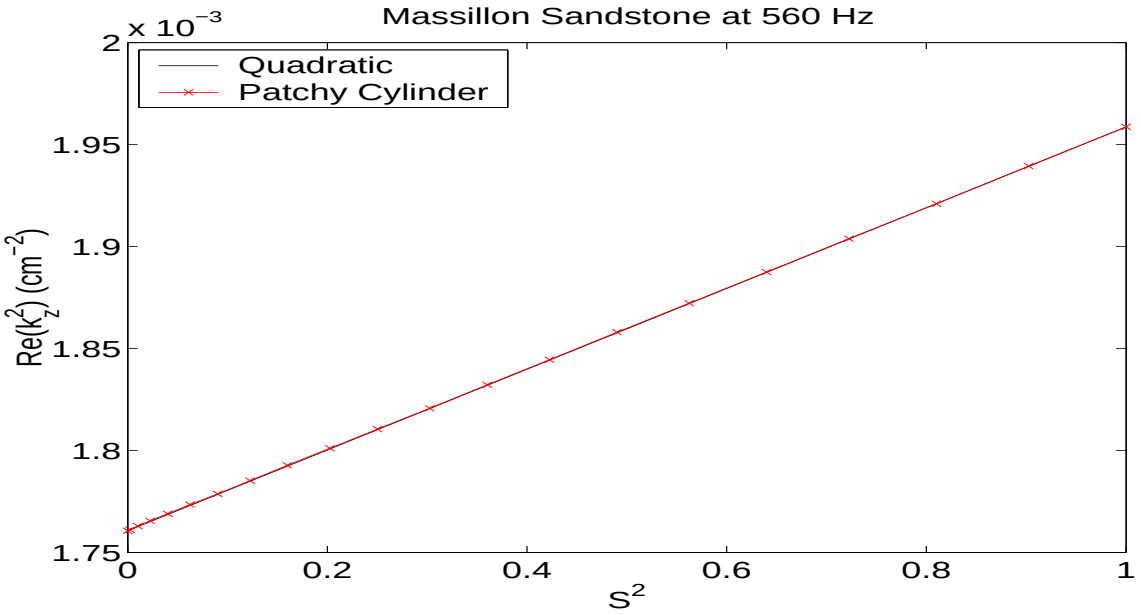

Figure 9: Comparison between the points that solve the dispersion relation in the complex k_z^2-plane, and a simple quadratic fit in water saturation S, for the Massillon sandstone measured by Murphy. The fit is nearly perfect for this case. jim2-ms_quadratic [NR]

Biot, M. A., 1956a, Theory of propagation of elastic waves in a fluid-saturated porous solid. I. Low-frequency range: *J. Acoust. Soc. Am.* **28**, 168–178.

Biot, M. A., 1956b, Theory of propagation of elastic waves in a fluid-saturated porous solid. II. Higher frequency range: *J. Acoust. Soc. Am.* **28**, 179–1791.

Biot, M. A., 1962, Mechanics of deformation and acoustic propagation in porous media: *J. Appl. Phys.* **33**, 1482–1498.

Chin, R. C. Y., Berryman, J. G., and Hedstrom, G. W., 1985, Generalized ray expansion for pulse propagation and attenuation in fluid-saturated porous media: *Wave Motion* **7**, 43–66. |item Chree, C., 1886, Longitudinal vibrations of a circular bar: *Quart. J. Pure Appl. Math.*, **21**, 287–298.

Deresiewicz, H., and Skalak, R., 1963, On uniqueness in dynamic poroelasticity: *Bull. Seismol. Soc. Am.*, **53**, 783–788.

Gassmann, F., 1951, Über die elastizität poröser medien: *Vierteljahrsschrift der Naturforschenden Gesellschaft in Zürich*, **96**, 1–23.

Hadley, K., 1976, Comparison of calculated and observed crack densities and seismic velocities in Westerly granite: *J. Geophys. Res.* **81**, 3484–3494.

Hashin, Z., and Shtrikman, S., 1961, Note on a variational approach to the theory of composite elastic materials: *J. Franklin Inst.* **271**, 336–341.

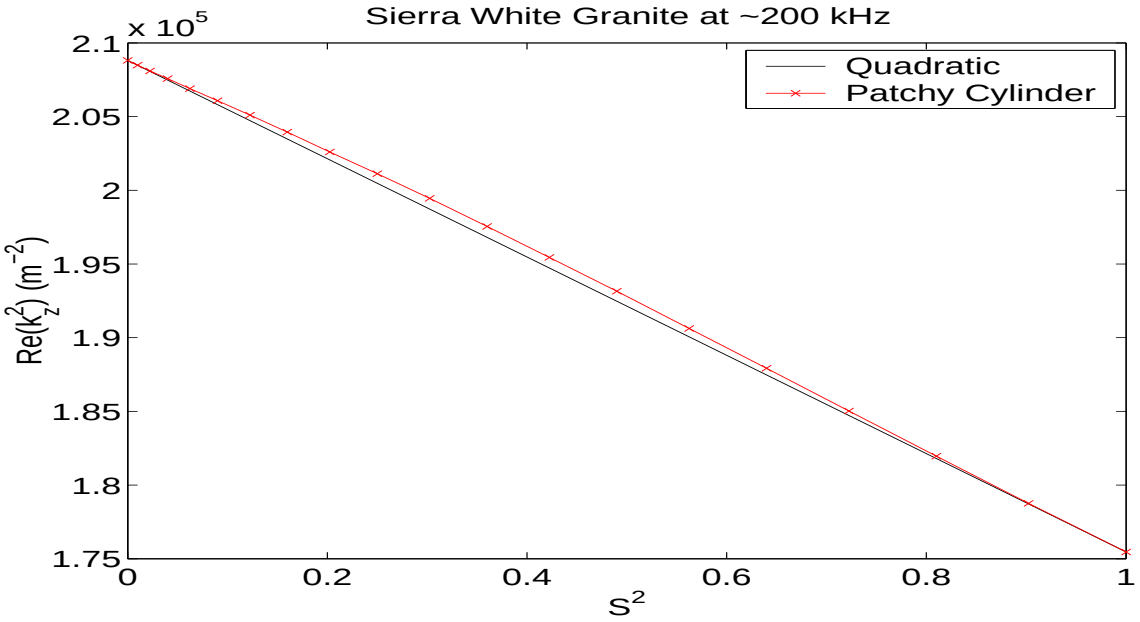

Figure 10: Comparison between the points that solve the dispersion relation in the complex k_z^2-plane, and a simple quadratic fit in water saturation S, for the Sierra White granite measured by Murphy. The fit is also good for this case, but not as good as it was for Massillon sandstone. jim2-swg_quadratic [NR]

Hashin, Z., and Shtrikman, S., 1962, A variational approach to the theory of elastic behaviour of polycrystals: *J. Mech. Phys. Solids* **10**, 343–352.

Johnson, D. L., 2001, Theory of frequency dependent acoustics in patchy-saturated porous media: *J. Acoust. Soc. Am.* **110**, 682-694.

Knight, R., and Nolen-Hoeksema, R., 1990, A laboratory study of the dependence of elastic wave velocities on pore scale fluid distribution: *Geophys. Res. Lett.* **17**, 1529–1532.

Milton, G. W., 1985, The coherent potential approximation is a realizable effective medium scheme: *Comm. Math. Phys.* **99**, 463–500.

Murphy, William F., III, 1982, *Effects of Microstructure and Pore Fluids on the Acoustic Properties of Granular Sedimentary Materials*, Ph.D. Dissertation, Stanford University.

Pochhammer, L., 1876, Über Fortpflanzungsgeschwindigkeiten kleiner Schwingungen in einem unbegrenzten isotropen Kreiscylinder: *J. Reine Angew. Math. (Crelle)*, **81**, 324–336.

Pride, S. R., and Flekkoy, E. G., 1999, Two-phase flow through porous media in the fixed-contact-line regime: *Phys. Rev. E*, **60**, 4285–4299.

Pride, S. R., Tromeur, E., and Berryman, J. G., 2002, Biot slow-wave effects in stratified rock: *Geophysics*, **67**, 271–281.